https://doi.org/10.1017/S155192950005433X Published online by Cambridge University Press

Imaging Carbon Nanoparticles in Cells

Mhairi Gass* and Alexandra Porter**
*SuperSTEM, Daresbury Laboratory, Daresbury, U.K.
**Imperial College London, London, U.K.
m.h.gass@liv.ac.uk

The application of nanotechnology in disciplines as varied as medicine and electronics is advancing rapidly with carbon nanoparticles (CNPs) such as fullerenes (C_{60}) and nanotubes at the forefront. However, a lack of understanding of the interaction of such small structures with cellular material has resulted in concerns over their impact on human health [1-3] and since the individual structures have a diameter of ~1 nm they are potentially small enough to penetrate through ion channels or diffuse through pores in the nuclear membrane. Assessing their toxicity is imperative. In response to these concerns there has been an increase in the number of papers addressing the toxicity of carbon nanoparticles over the last few years but much of this data appears contradictory [1-6]. It is therefore essential to understand how the human body interacts with CNPs and more specifically to elucidate pathways by which CNPs enter the cell and their distribution within.

Transmission electron microscopy (TEM) is a powerful technique for imaging nanoparticles; however, due to the inherently small size of such particles, combined with their similar elemental composition to that of the cell, traditional TEM methods are limited. It is therefore necessary to combine experience from the TEM communities in both biological and physical sciences to enable a full characterisation of CNPs in cellular structures to determine mechanisms of transport across the cell membrane, interactions with the membranes and organelles and their distribution within the cell - knowledge of which is fundamental to understand any potential toxicity. In this report, we will discuss a range of methods developed to image CNPs in cellular structures using TEM—from lower resolution tomography of CNP aggregates in whole cells to high-resolution visualisation of individual single wall nanotubes within the cell. We will also review the preparation of samples to optimise the data obtained from each technique.

How can we image CNPs in cellular structures?

While atomic resolution imaging in electron microscopy has become routine in the physical sciences, in the biological sciences, although the desire for higher resolution exists, the emphasis has necessarily concentrated on low dose to minimise specimen damage. Standard TEM techniques such as bright field imaging of cellular structures result in very weak contrast; traditionally, researchers have stained the cells with heavy metal stains to enhance the cellular structure, however this leads to confusion between stain artefacts and CNPs when analysing the samples at high magnification. Further, standard sample thicknesses for TEM sections can vary from 70nm to several hundred nanometres. This results in the acquisition of a 2D image containing 3D information, as demonstrated by the drawing in Figure 1, which can, in turn, result in the "blurring" of data or lack of information. Although it is necessary to look at stained samples to determine the morphology of the cells, the techniques described in this work mainly concentrate on enhancing contrast between CNPs and the cell of unstained sections. The techniques can be split into two parts: 1. medium resolution imaging to gain an overall picture of the location of CNPs in cells and 2. high resolution imaging to image individual CNPs within the cell. The former will look at high angle annular dark field (HAADF) imaging and energy filtered TEM (EFTEM) and discuss their suitability for tomography using a standard (S)TEM such as an FEI Tecnai F20. The latter will look at the combination of HAADF, electron energy loss spectroscopy (EELS) and bright field imaging in SuperSTEM, a dedicated aberration corrected scanning transmission electron microscope (STEM), to image individual single wall nanotubes (SWNTs) within the cellular structure.

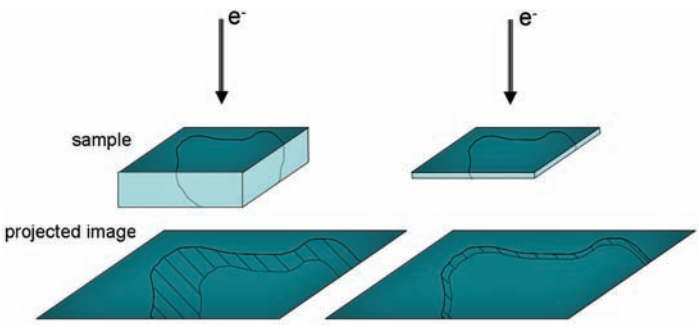

Figure 1. Drawing showing blurring of information when acquiring a projection of a 2D image from a thick 3D section compared to a thinner section.

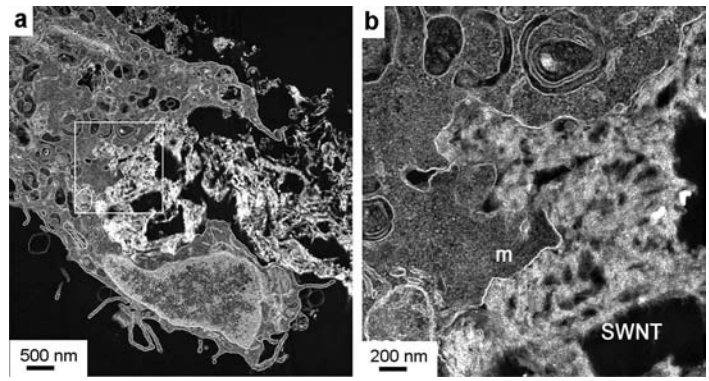

Figure 2. HAADF-STEM image of a stained sample showing SWNT bundles being actively ingested by a phagosome at 4 days. b, Higher magnification image of boxed area in image a illustrating that SWNTs were compartmentalized inside the phagosomal membrane (m). Figure first published by Porter et al in Nature Nanotechnology [7], Copyright (2007)

Sample preparation

One of the greatest challenges for imaging nanoparticles within cells is in the sample preparation. When preparing samples for TEM it is essential to induce minimal alteration to cell ultrastructures and to the distribution of nanoparticles within the cell. The techniques used in this work are described below.

Human monocyte derived macrophage were treated with C_{60} for 24 h and with SWNTs for 2 and 4 days at concentrations of 5 μg/ml in cell culture medium. Following exposure, washed cell monolayers were fixed with 4% glutaraldehyde in PIPES buffer (0.1 M, pH 7.4) for 1 h at 4 °C. Then, cells were treated with graded solutions of ethanol (70, 95, and 100%) for 5 min in each solution. Samples were infiltrated under vacuum in LR white resin for 3 days. Samples were then cured in fresh LR white for 23 h at 60 °C 1. Sections were cut onto distilled water with an ultramicrotome using a 35° wedge angle diamond knife and collected immediately on TEM grids and dried for an hour at 37 °C. For whole-cell samples macrophages exposed to C_{60}, seeded on formvar coated gold grids, were cryo-immobilized by rapid immersion into liquid propane cooled by liquid nitrogen. Gold

1 If stained sections are required, the sample should be set in quetol resin rather than LR white used for unstained sections. The cells are treated with osmium tetroxide, bulk stained with uranyl acetate and the sections are post-stained with uranyl acetate and lead citrate for 5 min in each to enhance contrast from cell membranes and organelles.

https://doi.org/10.1017/S155192950005433X Published online by Cambridge University Press

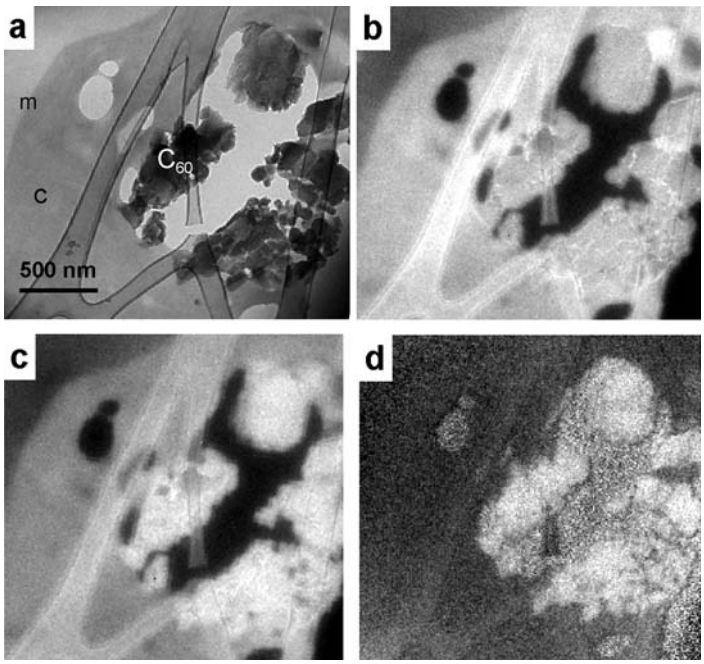

Figure 3. EFTEM images of cell exposed to C_{60}. (a) 0 eV, (b) 20 eV, (c) 26 eV, (d) 26/20 eV, using a 2eV slit of crystals of C_{60} within a lysosome. Clusters in the 26 eV image have a higher intensity than the cell medium in the 26 eV image than in the 20 eV image, and this increase in intensity is confirmed in the ratio image (26 eV/20 eV) in part d. m - plasma membrane, c - cytoplasm. Reprinted in part with permission from Ref 9. Copyright (2007) American Chemical Society.

and not copper grids were used as copper is toxic to the cultured cells. The samples were freeze-dried by raising the temperature to room temperature over 24 h at a pressure of $5x10^{-6}$ bar.

1. Locating CNPs in cells at medium resolution

i) HAADF STEM

HAADF STEM uses an annular detector to collect electrons which have been scattered to high angles, where the intensity is proportional to the mass-density, with a relationship to the atomic number of $\sim Z^{1.7}$. This technique may be used to image the distribution of SWNTs and C_{60} clusters within cells at medium resolution as the crystalline nanoparticles are denser than the surrounding cell, resulting in more intensity in the image. HAADF imaging is particularly suited to SWNTs as there are surface iron catalyst particles, which scatter strongly due to their higher atomic number, producing enhanced contrast [7] as well as stained sections where the heavy metals scatter strongly. Figure 2 demonstrates the bright contrast achieved from a stained section where SWNT bundles are clearly identifiable from the surrounding cell [8,9,7]. The contrast achieved in HAADF imaging is much greater than traditional bright field imaging where it is very difficult to distinguish the carbon nanostructures within unstained cells, this furthers our understanding of how these structures interact with cell organelles.

ii) EFTEM

EFTEM is an imaging technique often used in the physical sciences where the image is made up of transmitted electrons that have lost a known energy. A brief description as to how the electrons lose specific energies to the specimen follows.

As the incident electrons pass through the specimen most of them are elastically scattered (i.e. they lose no energy to the sample) while the remainder are inelastically scattered, ionizing core-level atomic electrons at energies characteristic to the elements present. Another feature that appears in the low-loss part of the energy loss spectrum

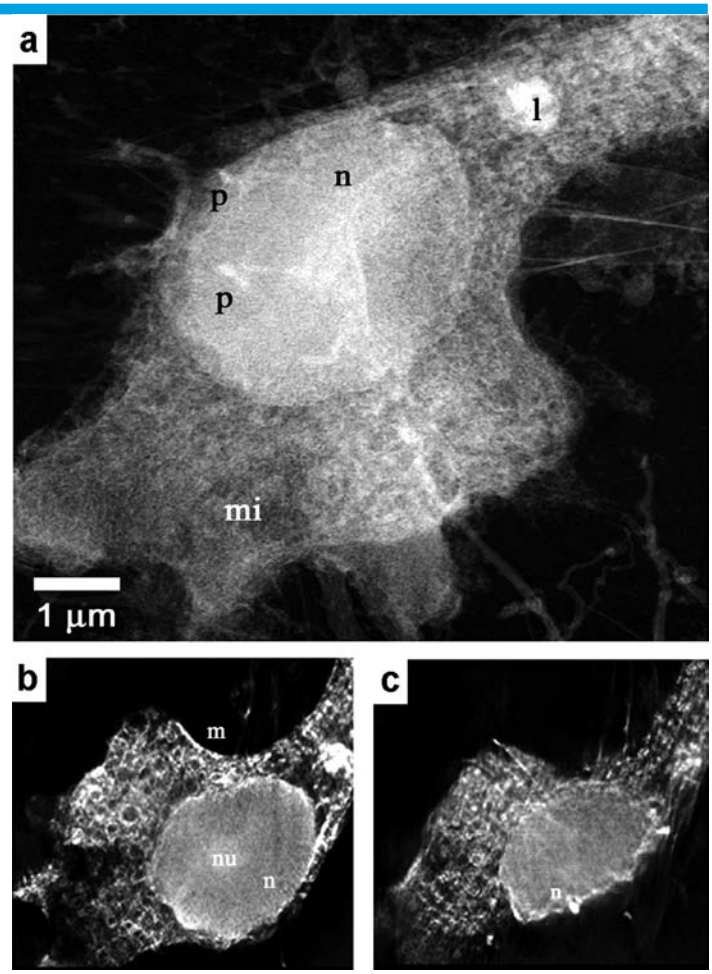

Figure 4. HAADF tomography of a freeze-dried whole cell exposed to C_{60} for 24h. a) the cell at imaged at zero tilt illustrating particles (p) within the lysosomes (l) and associated with the nucleus. A series of horizontal (b–d) slices through the reconstructed tomogram illustrate membranes (m), the nucleus (n), the cytoplasm (c) and secondary lysosomes (l). Reprinted from Porter et al 'Uptake of C_{60} by human monocyte macrophages, its localization and implications for toxicity: Studied by high resolution electron microscopy and electron tomography' [8], Copyright (2006), with permission from Elsevier.

of carbon is the $(\pi+\sigma)$ volume plasmon that results from the interaction of the incident electrons with the outer-shell atomic electrons. The low-loss region of the energy loss spectrum has two advantages for imaging carbonaceous species: (i) the scattering cross-sections are many orders of magnitude larger than for core-loss scattering, and thus acquisition times and beam damage can be minimized, and (ii) the $(\pi+\sigma)$ volume plasmon excitation, which dominates the low-loss spectrum, is sensitive to the electronic structure of the carbon species[2]. In the low-loss spectrum, C_{60} and SWNTs exhibit a bulk plasmon energy, arising from oscillations of the π and σ electrons, of around 26 eV, whereas amorphous carbon exhibits a plasmon energy of ~23 eV. Graphitic-like carbonaceous materials also exhibit an interband $\pi \rightarrow \pi^*$ transition at 6 eV. This $\pi \rightarrow \pi^*$ transition results from the excitation of electrons in the π bond and is therefore very weak or missing in the amorphous material.

The combination of fast acquisition and sensitivity to material

2 The plasmon is a collective oscillation of the loosely bound valence electrons that can be estimated by the free-electron model as $E_p = \hbar\sqrt{\frac{ne^2}{m\varepsilon_0}}$, where n is the valence electron density, e the elementary charge, m the electron mass and ε_0 the permittivity of free space; it follows that the plasmon energy for materials of similar composition is dependant on their density.

Beating the Competition is Easy, When You've Got Products They Don't Offer!

Si-Li EDS Detectors,
IXRF offers guaranteed, premium ≤ 130eV, resolution Si-Li detectors. *(*industry standard detector resolution 133-138eV)* that carry a three year warranty.

New 30mm^2 at 133eV, three year warranty available for cost effective fast X-ray Mapping.

X-Beam, Micro XRF,
40-60 micron spot. 10,000 times more analytically sensitive than EDS. Out performs WDX for less than half the cost.

fX SEM XRF,
400-1000 micron spot. 10,000 times more analytically sensitive than EDS.
Perfect for environmental applications as well as non-conductive samples.

50mm^2 Silicon Drift Detector, the largest Active Area in the industry (50mm^2). 133eV resolution, with optimum peak stability, and high input count rates. Who says "Bigger isn't better"?

IXRF does not stratify their software suite into low, medium, and high-end levels; there's only one high-end package that includes a myriad of Spectra Analysis, Image Analysis, X-ray Mapping, and unsurpassed SEM/EDS Automation.

Free Software Upgrades for Life…no compromises.

IXRF SYSTEMS

IXRF Systems, Inc. 15715 Brookford Dr, Houston, Texas, 77059 (Tel): 281/286-6485 (Fax): 281/286-2660
www.ixrfsystems.com

density makes the plasmon feature an ideal candidate for imaging CNPs in cellular structures. It is however essential that the sample is not stained as the stain will alter the chemical composition of the section; hence alter the information in the energy loss spectrum.

By selecting an energy-filter slit that only allows electrons through that have lost certain energies, elemental EFTEM maps can be produced - and acquisition of an extended series of images over the energy loss region of interest can produce fully quantitative elemental maps [10]. When acquiring EFTEM images it is necessary to have an objective aperture in to enhance contrast and maintain sample stability, in this case an objective aperture of 10μm was used. Using EFTEM we have been able to image the plasma membrane, nucleus and lysosomes by imaging with a 2eV energy filter centred on the two volume plasmon energies for the different carbon species, contrast between the cell and the CNPs is enhanced [7,9]. Figure 3a-c shows EFTEM images of cells exposed to C_{60} recorded around 0eV, 20eV and 26eV. The difference in volume plasmon energies between the cell and fullerene C_{60} allows a ratio of the EFTEM images (26eV / 20eV) to be used to differentiate the two carbonaceous materials, illustrated by the enhanced contrast from the C_{60} in Figure 3d. This technique can be extended to 3 dimensions as will be discussed below.

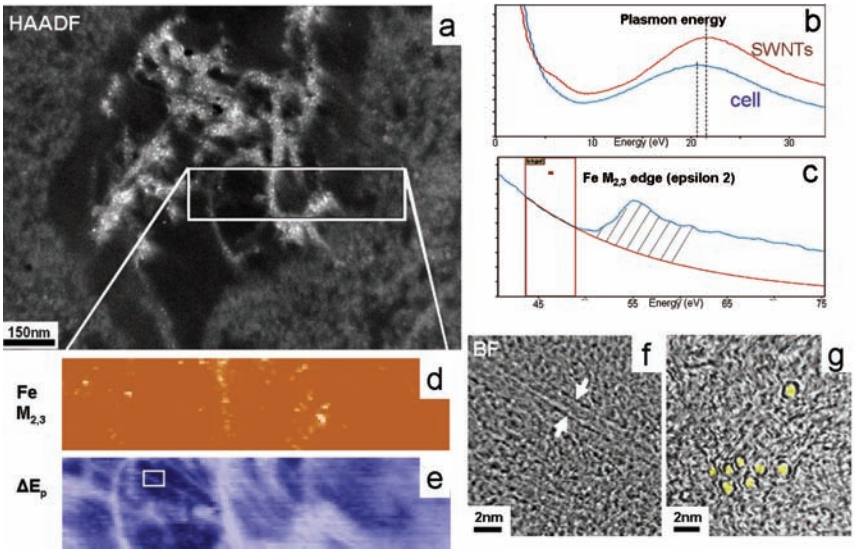

Figure 5. Aberration corrected STEM applied to image cells exposed to SWNTs for 2 days. a) location of SWNTs in a membrane enclosed vesicle at medium resolution using HAADF STEM; b) the low-loss EELS spectra from the cell alone and SWNTs in the cell show a small shift in plasmon energy; c) the iron edge extracted from the low loss spectrum which is integrated, the resulting iron map is shown in d) separating out the contribution from SWNTs and iron. Mapping the shift in plasmon energy results in e) where SWNTs can be identified for high resolution BF imaging f); g) another example of SWNTs end on in the sample, ends highlighted in yellow. Figure first published by Porter et al in Nature Nanotechnology [7], Copyright (2007).

iii) Electron tomography

Electron tomography is a 3D technique, which is key for understanding the organization and structure of inorganic and biological materials [11]. For example, in the life sciences, cryotomography is commonly used to analyze cellular structures, viruses and bacteria; in physico-chemical sciences, there is a need to understand the functional and mechanical behavior of materials in three dimensions at the nanoscale. For a detailed review of this technique the reader should refer to Midgley *et al.* [11]. The basis of the technique is the rotation of a specimen about a single axis, leading to the acquisition of an image over every 1–2°, typically in a tilt range of ± 70°. A back-projection algorithm, or similar, is then used to compute a 3D reconstruction of the specimen.

Electron tomography can be combined with either HAADF-STEM or EFTEM. The advantage of HAADF-STEM tomography is its suitability for imaging thick sections: The absence of a post-specimen imaging lens means the effects of chromatic aberration can be avoided, such that image contrast and resolution remain high. Using HAADF-STEM tomography, it is possible to image sections of up to 300 nm thickness with good resolution, even freeze-dried whole cells cultured on a TEM grid. Images of the reconstructed whole cell are shown in Figure 4 where the white features are aggregates of C_{60}, and clearly show the C_{60} within the cell but not in the nucleus.

EFTEM tomography is based on acquiring energy-filtered images over the energy loss of interest at every tilt. By acquiring an extended series of images over the energy loss region of interest for the tilt series, known as spectral tomography, chemical information from specific volumes of material can be extracted, enabling a far more accurate 3D characterization of carbonaceous nanocomposites, and indeed of many other nanoscale structures, than has previously been possible [12]. However, spectral tomography is limited for imaging carbon nanoparticles in cells, since long exposure times are required, with subsequent beam damage. By acquiring only two energy-filtered images over the π+σ plasmon energies the dose is kept down and by reconstructing data from ratio images of say 26eV / 20eV, it is possible to gain contrast between the graphitic CNPs and the cell. However, EFTEM tomography is limited to sample thickness, with 70nm thick sections used compared to 300nm thick sections for HAADF tomography.

2. Imaging at high resolution

Imaging of individual CNPs such as SWNTs within a cellular structure requires a combination of techniques. The knowledge acquired for locating CNPs at medium resolution discussed previously is combined and applied to a dedicated aberration corrected scanning transmission electron microscope fitted with electron energy loss spectroscopy (EELS), the microscope used in this work is the SuperSTEM, based in Daresbury, U.K.

i) Sample preparation

The first issue surrounding high resolution imaging is the specimen thickness. As demonstrated in Figure 1, in contrast to tomography where 3D information in the sample is a prerequisite, for high resolution imaging it is necessary to have the thinnest possible sample. Standard sample thicknesses for TEM sections can vary from 70nm to several hundred nanometres resulting in the acquisition of a 2D image containing 3D information which in turn can result in the "blurring" of data or lack of information. By cutting ultra-thin sections of around 20nm in thickness using an ultra-microtome, slices that are effectively 2D through cells are obtained, therefore minimising artifactual 3-dimensional information, allowing for high resolution imaging of unstained samples. The sections are put onto unsupported grids so that there is no contribution from an amorphous carbon support. Such thin, unsupported samples, combined with the focused beam used in STEM, in turn pose their own problems, namely their stability. Before the sections are analysed it is necessary to spread the electron beam over an area of the sample (e.g. a grid square) with the apertures removed. This exposes the sample to a low dose of

electrons and allows it to shrink gently[3] – if the beam were focused directly onto the sample without prior exposure the section would rip apart. The area can often require this treatment for several hours before the beam can be focused onto the specimen for microscope tuning and imaging.

ii) Locating the CNPs

HAADF imaging is used at medium resolution to locate the iron particles associated with the SWNTs, these stand out as bright features due to their higher atomic number compared to carbon as is demonstrated in Figure 5a, where a bundle of iron decorated SWNTs are in a membrane enclosed vesicle.

To achieve contrast between SWNTs and the cell low-loss EEL spectroscopy can be applied. Unlike EFTEM discussed previously, where an image is acquired over a specific energy range, in EELS the energy loss spectrum is acquired at every point over a user defined area; this allows for improved energy resolution with greater capacity for post acquisition spectral analysis and is useful where a more detailed spectral analysis is required.

Using a high energy dispersion of 0.1eV per channel the low-loss region covering -10eV to ~100eV was acquired over the boxed region indicated in Figure 5a. Figure 5b shows an example of a spectrum extracted from a pixel with the zero loss peak extending off the vertical axis on the left hand side; it is good practice to remove plural scattering from the spectrum using a Fourier-log deconvolution, this removes any changes in spectral information due to thickness. A further feature occurs at around 54eV, this is the Fe $M_{4,5}$ edge and appears weak as it sits on the tail of the more intense plasmon. Using the Kramers-Kronig procedure it is possible to extract epsilon 2 (ε_2), the imaginary part of the dielectric function, which represents the absorption of energy by optical transitions; as the plasmon is not a result of absorption, it is not present in ε_2 thus allowing for a better background fit to the Fe $M_{4,5}$ edge, Figure 5c. By fitting a background to the Fe $M_{4,5}$ edge and integrating the signal intensity over the selected edge region an iron map is produced (Figure 5d), this indicates the position of the iron catalyst particles with orange identifying no Fe and white identifying Fe particles - separating their contribution from that of the SWNTs.

Using the known shift in plasmon energy between the graphitic SWNTs and the amorphous carbonaceous cell a Gaussian can be fitted to the plasmon feature in the deconvoluted spectrum and the peak position extracted at every pixel in the map. The result is shown in Figure 5e where the false colour map shows areas of low plasmon energy in dark blue and areas where the plasmon energy is higher in white, this method is sensitive to very slight shifts in energy picking up the small shift in plasmon energy from a SWNT within the cell compared to the surrounding cell: the ratio technique described for EFTEM would not pick up such small shifts. The white features represent SWNTs and features are visible where there are no iron catalyst particles present as indicated by the boxed area, it is also noted that the feature indicated is not visible in the corresponding HAADF image. With an area containing SWNTs identified it is then possible to image them at higher magnification. While HAADF imaging has been useful at medium resolutions, at high magnification it becomes redundant for this material and the phase contrast bright field image is required. Figure 5f is a BF image taken from the area of interest defined with the plasmon map. It shows an individual SWNT running across the image, confirming that it is possible to image such small carbonaceous structures within cells. Figure 5g, taken from a different area, shows SWNTs end on that have been cut during sectioning, the SWNT ends have been highlighted in yellow and are part of a bundle that are piercing through a membrane.

3 Although the section shrinks under the beam due to mass loss this does not necessarily detract from the analysis as we are interested in the location of CNPs within the cell rather than the detailed structure of the cell itself.

Table 1. A summary of the different techniques used and their application to imaging carbon nanoparticles in cellular structures.

Technique	Objectives	Resolution / Specimen Thickness	Stained / unstained
BF	Identification of cellular structures	low - medium 70 nm	stained
HAADF	Detection of CNP aggregates	medium 70 nm	stained / unstained
HAADF tomography	Location of CNP aggregates in 3D	medium 300 nm	stained / unstained
EFTEM	Detection of CNP aggregates	medium 70 nm	unstained
EFTEM tomography	Location of CNP aggregates in 3D	medium 70 nm	unstained
STEM HAADF	Detection of CNP aggregates	medium - high 20 - 40 nm	unstained
STEM EELS	Detection of individual CNPs	medium - high 20 - 40 nm	unstained
STEM BF	Imaging of individual CNPs	high 20 - 40 nm	unstained

We have demonstrated that by combining a range of TEM techniques it is possible to image CNPs within stained and unstained cellular structures: at medium resolution to identify the larger aggregates using HAADF imaging and EFTEM and extending these to 3 dimensions, to imaging individual SWNTs with diameters of less than 1nm at high resolution. Care must be taken in optimising the sample for each technique and most importantly, patience is a necessity! ■

The authors would like to acknowledge Jeremy N. Skepper, Karin Muller, Paul A. Midgley and Mark Welland for their contributions.

References

1 Shvedova AA, Castranona V, Kisin ER, Schwegler-Berry D, Murray AR, Gandelsman VZ and Baron P, *J. Toxicol. Environ. Health A*, 2003, 66,1909

2 Manna SK, Sarkar S, Bar J, Wise K, Barrrera EV, Jejelowo O, Rice-Ficht A and Ramesh G, *Nano Lett.* 2005, 5(9),1676

3 Chui D, Tian F, Ozkan CS, Want M, Gao H, *Toxicol. Lett.* 2005, 155, 73

4 Worle-Knirsch JM, Pulskamp K and Krug HF, *Nano Lett.* 2006, 6(6),1261

5 Sayes CM, Liang F, Hudson JL, Mendez J, Guo W, Beach JM, Moore VC, Doyle CD, West JL,Billups WE, Ausman KD and Colvin VL, *Toxicol. Lett.* 2006, 161(2), 135

6 Nimmagadda, A, Thurston, K, Nollert, MU, McFetridge, PS, *J. Biomed. Mater. Res. A.* 2006, 1:76(3), 614

7 Porter AE, Gass M, Muller K, Skepper JN, Midgley PA and Welland M., *Nature Nanotechnology*, 2007, 2, 713

8 A. E. Porter, K. Muller, J. Skepper, P. Midgley, M. Welland, *Acta. Biomater.*, 2006, 2(4), 409-19.

9 A. E. Porter, M. Gass, K. Muller, J. N. Skepper, P. Midgley and M. Welland, *Environmental Science & Technology* 2007, 41, 3012

10 Thomas P. J. and Midgley P.A., *Ultramicroscopy*, 2001, 88(3), 179

11 Midgley PA, Ward EPWW, Hungría AB and Thomas JM., *Chem. Soc. Rev.*, 2007, 36, 1477

12 M. H. Gass, K. K. Koziol, A. Windle, P. Midgley, *Nano Letter* 2006, 6(3), 376-379